 CMES, vol.36, no.2, pp.173-191, 2008

Meshless Analysis of Ductile Failure

L. Li, S. Liu and H. Wang[1]

Abstract: We study ductile fracture using Reproducing Kernel Particle Interpolation and the Gurson-Tvergaard-Needleman (GTN) model. The meshless simulations are compared with the available experimental results and previous finite element simulations for crack propagation. The results agree well with experimental results, and it is confirmed that the proposed method provides a convenient and yet accurate means for simulation of ductile fracture.

Keyword: ductile fracture, meshless, GTN

1 Introduction

There is an enormous application potential for methods that are capable of predicting the onset and propagation of macroscopic cracks in structures undergoing gross plastic deformations. Despite a substantial effort over the past decades, still no method has been proposed which is fully satisfactory with regard to general accuracy on the one hand and ease of use for the engineering society on the other hand. One of the challenges in predicting fracture in structures is the significant span of length scales. While the size of structures is in the order of a meter the mechanics governing material separation under void growth and coalescence is on a scale of several micro-meters.

Typically, finite element methods are used for such type of problems. However, finite element methods are not well suited since in simulations of failure processes, we need to model the propagation of cracks with arbitrary and complex paths. Therefore, methods which can track the growth of extensive microcracking are required Belytschko and Tabbara (1996); Organ, Fleming, Terry, and Belytschko (1996); Fleming, Chu, Moran, and Belytschko (1997); Liu, Hao, and Belytschko (1999); Ventura, Xu, and Belytschko (2002); Rabczuk and Belytschko (2004); Hao, Liu, Klein, and Rosakis (2004); Chandra and Shet (2004); Hao, Liu, and Chang (2000); Maiti and Geubelle (2004); Rabczuk and Belytschko (2007).

[1] Department of Engineering Mechanics, Xi'an Jiaotong University, Xi'an, Shaanxi 710049, P.R. China

Meshless methods Atluri and Zhu (1998, 2000); Atluri and Shen (2002); Atluri (2002); Han and Atluri (2003); Tang, Shen, and Atluri (2003); Liu, Han, Rajendran, and Atluri (2006); Liu, Jun, and Zhang (1995a); Duarte and Oden (1996); Melenk and Babuska (1996); Belytschko, Lu, and Gu (1994, 1995); Rabczuk and Belytschko (2005); Idelsohn and Onate (2006); Hao and Liu (2006); Wu and Tao (2007); Wen and Hon (2007) are so far the most suited methods for dealing with this type of problems Rabczuk and Eibl (2003); Nishioka (2005); Guz, Menshykov, and Zozulya (2007); Hagihara, Tsunori, and Ikeda (2007); Nishioka, Kobayashi, and Fujimoto (2007); Guo and Nairn (2006a); Rabczuk and Areias (2006); Rabczuk, Areias, and Belytschko (2007); Rabczuk, Belytschko, and Xiao (2004); Ma, Lu, and Wang (2006); Gao, Liu, and Liu (2006a); Fujimoto and Nishioka (2006); Rabczuk, PMA, and Belytschko (2007); Rabczuk and Belytschko (2006); Chen, Gan, and Chen (2008); Zhang and Chen (2008); Guo and Nairn (2006b); Miers LS (2006); Gao, Liu, and Liu (2006b); Xu, Dong, and Zhang (2008); Wen, Aliabadi, and Lin (2008).

The basic idea is to resolve the continuum mechanics problem all the way to the crack tip and introduce material separation whenever a damage measure has reached a critical value. A very large number of constitutive models with evolving damage have been proposed over the past few decades. The simplest of these methods can be called damage indicators. Those methods do not include any coupling between the constitutive behavior and the material damage, except at the point of fracture where the stress carrying capacity is removed instantaneously. A large part of the methods falls in the category of damage mechanics, where a scalar or tensor defines the degradation of material stiffness without referring this damage quantity to the microstructure of the material. Finally, yet another category of methods uses micro-mechanics to relate the developing microstructure of the material to the macro-mechanical behavior of the material. The model applied in the present paper is based on the idea that material fracture is governed by nucleation, growth and coalescence of voids. The idea was originally proposed by Mc Clintock (1968) and Rice and Tracey (1969). It was further developed by Gurson (1977) and subsequently modified by Tvergaard (1981, 1982); Tvergaard and Needleman (1984). Although the model has certain shortcomings–see the discussions by Pardoen and Hutchinson (2000) and Roychowdhury, Roy, and Jr (2002) –it has also proved to be able to predict the important phenomena of initiation, Besson, Steglich, and Brocks (2001), and propagation Xia, Shih, and Hutchinson (1995); Kikuchi (2006). Since the focus of the present paper is on the application of the meshless method rather than on the material model, the Gurson-Tvergaard-Needleman (GTN) model is used here without modifications.

The paper is outlined as follows: We first state the governing equation. Then, we

develop the SPH formulation and apply the method to some problems. At the end, we conclude our paper.

2 Governing Equations

The governing equations are the continuity equation, momentum equation and energy equation. The energy equation is is only needed for problems involving heat transfer and related matters and is therefore not considered in our manuscript. For a Lagrangian description, conservation of mass (continuity equation is not required) can be written in an algebraic equation:

$$\rho_c J = \rho_0 \tag{1}$$

where ρ_0 and ρ_c are, respectively, the initial and current densities and J is the determinant of the deformation gradient, $J = det(\mathbf{F})$, $\mathbf{F} = \frac{d\mathbf{x}}{d\mathbf{X}} = \mathbf{I} - \frac{d\mathbf{u}}{d\mathbf{X}}$ where $\mathbf{I}$ is the second order unity tensor and $\mathbf{u}$ denotes the displacement field. Hence, the remaining equation is the momentum equation. In a Total Lagrangian description, conservation of linear momentum can be written as

$$\nabla_0 \cdot \mathbf{P} + \mathbf{b} = \rho_0 \ddot{\mathbf{u}} \in \Omega \tag{2}$$

where $\mathbf{b}$ is the body force per unit volume, superimposed dots denote material time derivatives and $\mathbf{P}$ is the first Piola-Kirchhoff stress tensor. The momentum equation is complemented with displacement and traction boundary conditions given as

$$\mathbf{u} = \bar{\mathbf{u}} \ on \ \Gamma_{0u} \tag{3}$$

$$\mathbf{n}_0 \cdot \mathbf{P} = \mathbf{t} = \bar{\mathbf{t}} \ on \ \Gamma_{0t} \tag{4}$$

where index t refers to "traction" and index u refers to "displacement"; $\mathbf{n}_0$ is the normal to the traction boundary.

3 Reproducing Kernel Particle Interpolation

We employ the reproducing kernel particle (RKP) interpolation Liu, Jun, and Zhang (1995b) for the meshless approximation of the dependent variables in PDEs. The problem domain Ω is first discretized into a set of particles $(\mathbf{x}_1, \mathbf{x}_2, ..., \mathbf{x}_N)$, where $\mathbf{x}_I$ is the location of node I and N denotes the total number of particles. The unknown variable $\mathbf{u}(\mathbf{x}, t)$ of a PDE is approximated by

$$\mathbf{u}^h(\mathbf{x}, t) = \sum_{I=1}^{N} N_I(\mathbf{x}) \mathbf{u}_I(t) \tag{5}$$

where $\mathbf{u}^h(\mathbf{x},t)$ is the approximation of $\mathbf{u}(\mathbf{x},t)$, $N_I(\mathbf{x})$ are the RKP shape function and $\mathbf{u}_I(t)$ are the nodal parameters. In RKP interpolation, the shape function $N_I(\mathbf{x})$ has the form

$$N_I(\mathbf{x}) = c(\mathbf{x}, \mathbf{x}-\mathbf{x}_I)\Psi_a(\mathbf{x}-\mathbf{x}_I) \tag{6}$$

where $c(\mathbf{x}, \mathbf{x}-\mathbf{x}_I)$ is the correction function expressed as a linear combination of an n-th order monomial basis:

$$c(\mathbf{x}, \mathbf{x}-\mathbf{x}_I) = \mathbf{H}^T(\mathbf{x}-\mathbf{x}_I)\mathbf{b}(\mathbf{x}) \tag{7}$$

with $\mathbf{H}^T(\mathbf{x}-\mathbf{x}_I)$ containing the basis functions

$$\mathbf{H}^T(\mathbf{x}-\mathbf{x}_I) = (1 \; x-x_I \; y-y_I \; \ldots \; (y-Y_I)^n) \tag{8}$$

In Eq. (6), $\Psi_a(\mathbf{x}-\mathbf{x}_I)$ is a weighting function that defines the smoothness and locality of the approximation with a compact support measured by h. A commonly used kernel function is the cubic spline function:

$$\Psi_a(s) \quad = \quad \begin{cases} \frac{2}{3} - 4s^2 + 4s^3 & 0 \le s \le \frac{1}{2} \\ \frac{4}{3} - 4s + 4s^2 - \frac{4}{3}s^3 & \frac{1}{2} \le s \le 1 \\ 0 & s > 1 \end{cases} \tag{9}$$

with $s = \frac{\mathbf{x}-\mathbf{x}_I}{h}$. The coefficient vector $\mathbf{b}(\mathbf{x})$ in Eq. (7) is obtained by satisfying the following n-th order reproducing conditions:

$$x^k y^l = \sum_{I=1}^{N} N_I(\mathbf{x}) x_I^k y_I^l \tag{10}$$

where $k+l = 0,1,2,...,n$. The solution for coefficient vector $\mathbf{b}(\mathbf{x})$ is obtained by substituting Eq. (6) into Eq. (10) yielding:

$$\mathbf{M}(\mathbf{x})\mathbf{b}(\mathbf{x}) = \mathbf{H}(\mathbf{0}) \tag{11}$$

$$\mathbf{M}(\mathbf{x}) = \sum_{I=1}^{N} \mathbf{H}(\mathbf{x}-\mathbf{x}_I)\mathbf{H}^T(\mathbf{x}-\mathbf{x}_I)\Psi_{aI}(\mathbf{x}-\mathbf{x}_I) \tag{12}$$

Upon solving for $\mathbf{b}(\mathbf{x}) = \mathbf{M}^{-1}(\mathbf{x})\mathbf{H}(0)$, the RKP shape functions take the form:

$$N_I(\mathbf{x}) = \mathbf{H}^T(\mathbf{0})\mathbf{M}^1(\mathbf{x})\mathbf{H}(\mathbf{x}-\mathbf{x}_I)\Psi_a(\mathbf{x}-\mathbf{x}_I) \tag{13}$$

4 Discretization

The weak form of the linear momentum equation is: Find $\mathbf{u} \in \mathscr{U}$ and $\delta\mathbf{u} \in \mathscr{U}_0$ such that

$$\delta W = \delta W_{int} - \delta W_{ext} + \delta W_{kin} = 0 \tag{14}$$

with

$$\begin{aligned}
\delta W_{int} &= \int_{\Omega_0} \nabla_0 \delta\mathbf{u} : \mathbf{P}\, d\Omega_0 \\
\delta W_{ext} &= \int_{\Gamma_{0t}} \delta\mathbf{u} \cdot \bar{\mathbf{t}}_0\, d\Gamma_0 + \int_{\Omega_0} \delta\mathbf{u} \cdot \mathbf{b}\, d\Omega_0 \\
\delta W_{kin} &= \int_{\Omega_0} \rho_0 \delta\mathbf{u} \cdot \ddot{\mathbf{u}}\, d\Omega_0
\end{aligned} \tag{15}$$

with the approximation spaces $\mathscr{U}$ and $\mathscr{U}_0$ for the trial and test functions, respectively,

$$\begin{aligned}
\mathscr{U} &= \left\{\mathbf{u} | \mathbf{u} \in H^1,\ \mathbf{u} = \bar{\mathbf{u}}\ on\ \Gamma_u\right\} \\
\mathscr{U}_0 &= \left\{\delta\mathbf{u} | \delta\mathbf{u} \in H^1,\ \delta\mathbf{u} = 0\ on\ \Gamma_u\right\}
\end{aligned} \tag{16}$$

Introducing the test and trial functions into the weak formulation yields

$$\sum_{I=1}^{n} \delta\mathbf{u}_I \left\{ \sum_{J=1}^{n} - \int_{\Omega_0} \nabla_0 N_I \mathbf{P}\, d\Omega_0 + \int_{\Omega_0} N_I \mathbf{b}\, d\Omega_0 + \int_{\Gamma_{0t}} N_I \bar{\mathbf{t}}_0\, d\Gamma_0 + \int_{\Omega_0} \rho_0 N_I N_J \mathbf{u}\, d\Omega_0 \right\} = 0 \tag{17}$$

For each particle I, the following identity must hold

$$\sum_{J=1}^{n} \int_{\Omega_0} \nabla_0 N_I \mathbf{P}\, d\Omega_0 = \int_{\Omega_0} N_I \mathbf{b}\, d\Omega_0 + \int_{\Gamma_{0t}} N_I \bar{\mathbf{t}}_0\, d\Gamma_0 + \int_{\Omega_0} \rho_0 N_I N_J \mathbf{u}\, d\Omega_0 = 0 \tag{18}$$

Rewriting these equations in matrix form gives the final system of equations:

$$\mathbf{M}_{IJ} \ddot{\mathbf{u}}_J = -\mathbf{f}_I^{ext} + \mathbf{f}_I^{int} \tag{19}$$

with

$$\mathbf{M}_{IJ} = \int_{\Omega_0} \rho \mathbf{N}_I\, \mathbf{N}_J^T\, d\Omega_0$$

$$\mathbf{f}_I^{ext} = \int_{\Gamma_{0t}} \mathbf{N}_I^T \, \bar{\mathbf{t}}_0 d\Gamma_0 + \int_{\Omega_0} \mathbf{N}_I^T \, \mathbf{b} d\Omega_0 \tag{20}$$

$$\mathbf{f}_I^{int} = \int_{\Omega_0} \nabla_0 \mathbf{N}_I^T \, \mathbf{P} d\Omega_0 \tag{21}$$

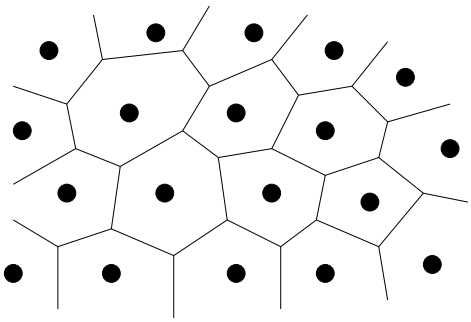

Figure 1: Voronoi cell diagram

The most efficient way to evaluate the integrals is nodal integration that results in a truly meshless method. In nodal integration, the particles are used as quadrature points and the associated integration weights are their tributary volumes obtained usually from Voronoi diagram, figure 1:

$$\mathbf{M}_{IJ} = \sum_{K=1}^{n} \rho_K N_I N_J V_K \tag{22}$$

$$\mathbf{f}_I^{ext} = \sum_{K=1}^{n} \mathbf{N}_I^T \, \mathbf{b}_K V_K + \sum_{K=1}^{n} \mathbf{N}_I^T \, \bar{\mathbf{t}}_{K0} A_K \tag{23}$$

$$\mathbf{f}_I^{int} = \sum_{K=1}^{n} \nabla_0 \mathbf{N}_I^T \, \mathbf{P}_K V_K \tag{24}$$

Since nodal integration leads to numerical instability due to numerical under-integration, several techniques have been developed Chen, Wu, Yoon, and You (2001); You, Chen, and Voth (2002). We employ stress-point integration and add additional

quadrature points to the nodes Randles and Libersky (2000). More detailed can be found e.g. in Randles and Libersky (2000).

Crack propagation is modeled by visibility method Belytschko, Lu, and Gu (1995). Therefore, discontinuities are introduced in the shape functions. The crack is described as line segments connected to each other. They can be inserted arbitrarily. An initial crack is propagated once the damage has reached a critical value ahead of the crack tip. Then, the crack line is extended in the direction of this particle. For sake of simplicity, we control the crack size of the crack advance vector and assume constant crack length when crack propagates.

5 Constitutive model

The Gurson-Tvergaard-Needleman (GTN) model is based on additive split of the rate-of-deformation tensor $\mathbf{D} = \mathbf{D}^{el} + \mathbf{D}^{pl}$. The Jaumann rate of the Cauchy stress tensor σ is used in the present formulation:

$$\sigma^{\nabla} = \mathbf{C} : \mathbf{D}^{el} = \mathbf{C} : \left(\mathbf{D} - \mathbf{D}^{pl}\right) = \sigma^{el} - \mathbf{C} : \mathbf{D}^{pl} \tag{25}$$

where $\mathbf{C}$ is the first order elasticity tensor. Objective trial stress is calculated making use of Hughes and Winget (1980) formula

$$\sigma_{n+1}^{el} = \mathbf{Q}\ \sigma_n\ \mathbf{Q}^T + \Delta t\ \mathbf{C}^{\nabla} : \mathbf{D} \tag{26}$$

with $\mathbf{Q} = \mathbf{I} + (\mathbf{I} - \alpha\mathbf{W})^{-1}\,\mathbf{W}$ where $\mathbf{I}$ is the second order identity matrix, $\mathbf{W}$ is the antisymmetric part of the velocity gradient and the parameter $\alpha = 0.5$. Note that the global integration scheme assumes constant first-order derivatives throughout the time step, which is consistent with the above assumption of constant values of $\mathbf{Q}$ and $\mathbf{W}$ during the time step. An interesting paper on objectivity of incremental constitutive formulations is discussed in detail in Rubenstein and Atluri (1983). The stress tensor can be decomposed into

$$\sigma = p\,\mathbf{I} + \frac{2}{3}\sigma_{eq}\,\mathbf{m} \tag{27}$$

with

$$p = \frac{1}{3}\sigma : \mathbf{I} \tag{28}$$

$$\sigma_{dev} = \sigma - p\mathbf{I} \tag{29}$$

$$\sigma_{eq} = \left(\frac{3}{2}\sigma_{dev} : \sigma_{dev}\right)^{1/2} \tag{30}$$

$$\mathbf{m} = \frac{3}{2\sigma_{eq}}\sigma_{dev} \tag{31}$$

where p denotes the hydrostatic stress and the index dev and eq denote deviatoric and equivalent stresses, respectively. The inelastic behavior of the material is described by a plasticity model which includes void growth caused by hydrostatic tension. The basic idea is that the state of the material damage is described by the current void volume fraction f , i.e. the volume of voids to the total element volume in a representative volume element. The material between the voids, i.e. at the microscopic level, is assumed to follow a general, isotropic material hardening law $f_h(\bar{\varepsilon}_{pl})$ where $\bar{\varepsilon}_{pl}$ is the microscopic plastic strain that is described by a power law

$$\bar{\sigma}_0 = f_h(\bar{\varepsilon}_{pl}) = \sigma_y \left(1 - \frac{E}{\sigma_y}\bar{\varepsilon}_{pl}\right)^N \tag{32}$$

where σ_y is the initial yield stress. The evolution of $\bar{\varepsilon}_{pl}$ is obtained from the physical condition that plastic work of the macroscopic stresses and strains should be equal to the energy dissipated in plastic deformations at micro-level

$$(1-f)\bar{\sigma}_0\ \dot{\bar{\varepsilon}}_{pl} = \sigma : \mathbf{D}^{pl} \tag{33}$$

which yields

$$\dot{\bar{\varepsilon}}_{pl} = \frac{\sigma : \mathbf{D}^{pl}}{(1-f)\bar{\sigma}_0} \tag{34}$$

At the macroscopic level, the yield function is given as

$$\phi = \left(\frac{\sigma_{eq}}{\bar{\sigma}_0}\right)^2 + 2a_1\ f^*(f)\ cosh\left(\frac{3a_2 p}{2\bar{\sigma}_0}\right) - \left(1 + a_1^2 f^*(f)^2\right) \tag{35}$$

where a_1 and a_2 are material parameters. When $f = 0$, the Gurson model obviously reduces to J_2 plasticity. The function $f^*(f)$ accounts for rapid void coalescence at failure and is given as

$$f^*(f) = \begin{cases} f & f \le f_c \\ f_c + \frac{1/a_1 - f_c}{f_f - f_c}(f - f_c) & f_c < f \le f_f \\ \frac{1}{a_1} & f > f_f \end{cases} \tag{36}$$

The void volume grows partly due to the expansion of existing voids and partly due to the nucleation of new voids:

$$\dot{f} = \dot{f}_{growth} + \dot{f}_{nucleation} \tag{37}$$

For incompressible material, the growth rate is

$$\dot{f}_{growth} = (1-f)\mathbf{D}^{pl} : \mathbf{I} \tag{38}$$

and the nucleation rate is described by the empirical relationship

$$\dot{f}_{nucleation} = A_N \dot{\bar{\varepsilon}}_{pl} \tag{39}$$

where we used the formulation by Chu and Needleman (1980)

$$A_N(\bar{\varepsilon}_{pl}) = \frac{f_N}{s_N\sqrt{2\pi}} exp\left(-0.5\left[\frac{\bar{\varepsilon}_{pl}-\varepsilon_N}{s_N}\right]^2\right) \tag{40}$$

with f_N being the volume fraction of void nucleating particles. As discussed e.g. by Tvergaard (1990); Roy and Jr (2002), the macroscopic material behavior during void initiation, growth and coalescence may exhibit a sensitivity to the shape and distribution of voids which cannot be captured by the void volume fraction alone. Even if the predicted value of f may not correspond to the measured value, several studies have shown that the model has excellent capacity to predict macroscopic behavior, i.e. crack length, applied loads, etc. Besson, Steglich, and Brocks (2001); Xia, Shih, and Hutchinson (1995); Xia and Shih (95a,b). From equation (35), it is seen that as the void volume fraction f grows towards f_f and $f^*(f)$ approaches $1/a_1$, the yield surface for the macroscopic stresses shrinks towards a point. To attain numerical stability the present procedure assumes full material damage, i.e. $\sigma = \mathbf{0}$, when $f = k_f f_f$ where $0.5 < k_f < 0.9$, as discussed later. The flow rule gives

$$\mathbf{D}^{pl} = \dot{\lambda}\frac{\partial\phi}{\partial\sigma} = \dot{\lambda}\left(\frac{\partial\phi}{3\partial p}\mathbf{I} + \frac{\partial\phi}{\partial\sigma_{eq}}\mathbf{Im}\right) \tag{41}$$

Defining

$$D_p = \dot{\lambda}\left(\frac{\partial\phi}{3\partial p}\right) \ , \ D_{eq} = \left(\frac{\partial\phi}{\partial\sigma_{eq}}\mathbf{I}\right) \tag{42}$$

the flow rule finally writes

$$\mathbf{D}^{pl} = \frac{1}{3}D_p\,\mathbf{I} + D_{eq}\mathbf{m} \tag{43}$$

Elimination of $\dot{\lambda}$ in equation (42) gives

$$D_p\,\frac{\partial\phi}{\partial\sigma_{eq}} + D_{eq}\frac{\partial\phi}{\partial p} = 0 \tag{44}$$

By inserting equation (43) back into equation (26) and integrating from t_n to t_{n+1}, one can show that the relaxation from the trial stress is given by

$$\sigma_{n+1} = \sigma_{el} - K\,\Delta t\,D_p\,\mathbf{I} - 2G\,\Delta t\,D_{eq}\,\mathbf{m}_{n+1} \tag{45}$$

The mean and equivalent components of this equation are

$$\sigma_m = \sigma_m^{el} - K\,\Delta t\,D_p\ ,\ \ \sigma_{eq} = \sigma_m^{el} - 3G\,\Delta t\,D_{eq} \tag{46}$$

The underlying assumption of constant values of D_p and D_{eq} during the time step is consistent with the global, explicit integration method. Obviously, the return in deviatoric stress space is along $\mathbf{m}_{n+1}$ which can be determined from the trial stress tensor:

$$\mathbf{m}_{n+1} = \frac{3}{2\sigma_{eq}^{el}}\sigma_{dev}^{el} \tag{47}$$

The fact that $\mathbf{m}_{n+1}$ is determined by the elastic trial stress tensor simplifies the analysis significantly because the stress tensor at t_{n+1} is then determined by only two unknowns, (D_p, D_{eq}), instead of all six components of the stress tensor. For the constitutive update, we proceed as follows: Consider the two internal variables, the effective plastic strain and the void volume fraction. The time derivatives of these internal variables are given by equations (34) and (35):

$$\frac{\partial \bar{\varepsilon}^{pl}}{\partial t} = \frac{p\mathbf{D}_p + \sigma_{eq}\mathbf{D}_{eq}}{\sigma_0(1-f)} \tag{48}$$

$$\frac{\partial f}{\partial t} = (1-f)\mathbf{D}_p + A_N\frac{\partial \bar{\varepsilon}^{pl}}{\partial t} \tag{49}$$

Integration in time is then simply given by

$$\bar{\varepsilon}_{n+1}^{pl} = \bar{\varepsilon}_n^{pl} + \Delta t\,\frac{\partial \bar{\varepsilon}^{pl}}{\partial t} \tag{50}$$

$$f_{n+1} = f_n + \Delta t\,\frac{\partial f}{\partial t} \tag{51}$$

In order to determine the values of D_p and D_{eq} which satisfy the yield function and the flow rule at t_{n+1} an iterative Newton method is used. Equations 35 and 44 to be solved are denoted by g_1 and g_2, respectively:

$$\begin{aligned} g_1(D_p, D_{eq}) &= \phi(D_p, D_{eq}) = 0 \\ g_2(D_p, D_{eq}) &= D_p\,\frac{\partial \phi}{\partial \sigma_{eq}} + D_{eq}\frac{\partial \phi}{\partial p} = 0 \end{aligned} \tag{52}$$

where the index '$n+1$' is dropped for simplicity. The roots (D_p, D_{eq}) are determined in a predictor-corrector iteration by improving the initial, predicted estimate, (D_p^k, D_{eq}^k)

$$\begin{aligned} D_{eq}^{k+1} &= D_{eq}^k + \Delta D_m^k \\ D_p^{k+1} &= D_p^k + \Delta D_p^k \end{aligned} \tag{53}$$

where k is an iteration counter. The correction $(\Delta D_p^k, \Delta D_{eq}^k)$ is found by a first-order Taylor expansion of g_1 and g_2 and solution of the resulting linearized set of equations:

$$\begin{aligned} g_1^{k+1} &= g_1^k + \frac{\partial g_1^k}{\partial D_p}\Delta D_p^k + \frac{\partial g_1^k}{\partial D_{eq}}\Delta D_{eq}^k = 0 \\ g_2^{k+1} &= g_2^k + \frac{\partial g_2^k}{\partial D_p}\Delta D_p^k + \frac{\partial g_2^k}{\partial D_{eq}}\Delta D_{eq}^k = 0 \end{aligned} \tag{54}$$

where the notion $g_i^k = g_i(D_p^k, D_{eq}^k)$ is employed.

6 Results

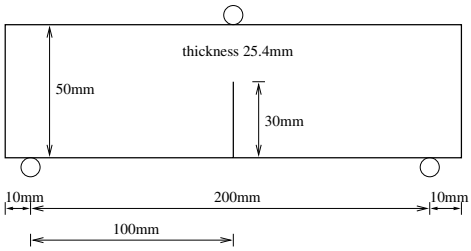

Figure 2: Three-point beam in bending

We consider the three-point test in bending. Experimental data is well documented Joyce and Hacket (1994); Joyce and Link (1994). There is also computational data Xia and Shih (95a), who employed the finite element method, pre-defined the crack path. Therefore, the crack is to be within a row of the so-called "computational cells", each with a constitutive behavior according to the GTN model. They choose a side length of the computational cells of 0.2mm and adjusted the material parameters of the GTN model to give a good prediction of the loads and crack growth in the TPB specimen.

We will use the same material parameters and the same particle spacing in our paper (as compared to Xia and Shih (95a)) but will also test coarser 'meshes' to demonstrate the capability of our method. Note that the crack path is not aligned in our simulation but can grow arbitrarily. This advantage can be better exploited for more complex phenomena. However, the purpose of our paper is to demonstrate the applicability of our approach to ductile fracture. The test-setup is illustrated in figure 2. The material parameters are: Young's modulus $E = 300$GPa, Poisson's

ratio $\nu = 0.3$, initial yield stress $\sigma_y = 400$MPa, hardening exponent $N = 10$, initial void volume ratio $f = 0.005$, void volume at coalescence $f_c = 0.021$, void volume at total failure $f_f = 0.2109$, parameters $a_1 = 1.5$ and $a_2 = 1.0$ and void nucleation parameter $f_N = 0$.

Symmetry conditions are not enforced, in order to allow the crack to move away from the symmetry line. We present results starting from around 80,000 (0.4mm particle spacing) particles up to more than 160,000 particles (0.2mm particle spacing):

- 0.2mm
- 0.3mm
- 0.4mm

In these simulations, a uniform particle spacing is used. We tested also discretizations with finer particle densities around the crack tip (from 0.4mm up to 0.1mm) and gradually coarsened the mesh. These simulations gave very similar results to the ones with uniform particle spacing. Note that the number of particle increases slightly during crack propagation when the crack propagates.

The essential boundary conditions are enforced by point collocation Gunther and Liu (1998). At the supports, displacement boundary conditions were enforced for only two particles (similar to Xia and Shih (95a)) and the essential boundary conditions at the loading point are prescribed over a length of approximately 2mm. This assures global bending mode of the beam rather than just a local indentation at the loading point. The displacement of the loading point is increased at a sufficiently low and smooth rate to ensure that dynamic effects do not dominate the response.

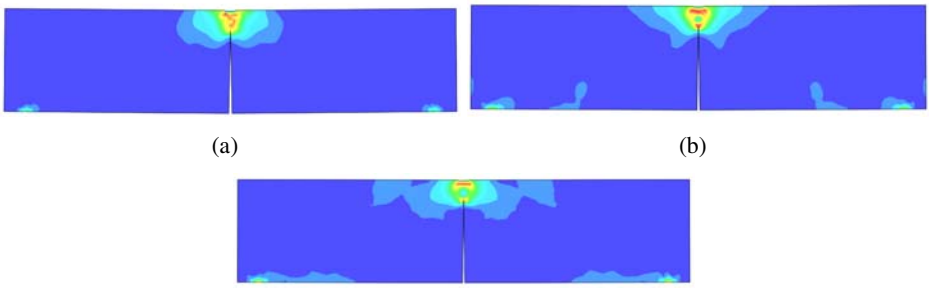

Figure 3: Displaced configuration of Three-point bending beam

Figure 3 shows sequences of the global bending of the beam together. Obviously, the load does introduce some local indentation but the figures also illustrate that the global bending is dominant, as it should be. Figure 4 shows a comparison between the present predictions and the experiments. We firstly note that the results are independent of mesh refinement. A particle spacing of 0.4mm is sufficient. Secondly, the agreement between experiment and numerical simulation is good and similar to the one obtained in Xia and Shih (95a). As the purpose of the paper is to demonstrate that our method can be used to predict ductile fracture, no attempts have been made here at carefully adjusting material- and numerical parameters to make a perfect fit to experiments. Figure 4b shows the predicted increase in crack length as a function of the displacement of the loading point. The experimental results presented by Joyce and Hacket (1994); Joyce and Link (1994) also showed a crack length of approximately 5mm when the displacement was 6.5mm, i.e. a result very close to the prediction shown in Figure 4b.

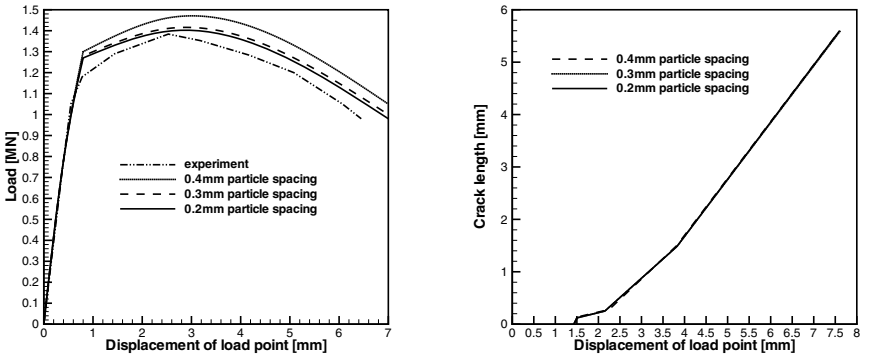

(a) (b)

Figure 4: a) Load displacement curve; b) Crack length displacement curve

7 Conclusions

We presented meshless method for prediction of ductile fracture under plane strain conditions. The Gurson-Tvergaard-Needleman model is adopted as the constitutive model. Crack propagation is modelled by the so-called visibility method. The visibility method modifies shape function in vicinity of the crack such that the displacement field becomes discontinuous.

We presented ductile fracture in a three-point bending beam with available experimental data Joyce and Hacket (1994); Joyce and Link (1994) that was tested by

other numerical method Xia and Shih (95a). Our computational results show that the proposed method seems to work well ductile crack propagation. Our results are in good agreement with the previously published experimental and numerical results. The next steps will be to develop this methodology for several propagating cracks and for crack nucleation. Crack nucleation is typically distinguished from crack propagation in meshfree method. Moreover, we intend to use novel techniques of modeling the crack through enrichment as e.g. suggested by Rabczuk and Zi (2007). Finally, the method will be extended to 3D.

It is thus believed that the proposed methodology could be further developed to become an accurate and practical procedure for modeling of ductile crack propagation.

References

Atluri, S. (2002): *The Meshless Local Petrov-Galerkin (MLPG) Method*. Tech Science Press.

Atluri, S.; Shen, S. (2002): The meshless local petrov-galerkin method: a simple and less-costly alternative to the finite element and boundary element methods. *Computations and Modelling in Engineering and Sciences*, vol. 3, pp. 11–51.

Atluri, S.; Zhu, T. (1998): A new meshless local petrov-galerkin (mlpg) approach in computational mechanics. *Computational Mechanics*, vol. 22, pp. 117–127.

Atluri, S.; Zhu, T. (2000): The meshless local petrov-galerkin (mlpg) approach for solving problems in elasto-statics. *Computational Mechanics*, vol. 25, pp. 169–179.

Belytschko, T.; Lu, Y.; Gu, L. (1994): Element-free galerkin methods. *International Journal for Numerical Methods in Engineering*, vol. 37, pp. 229–256.

Belytschko, T.; Lu, Y.; Gu, L. (1995): Crack propagation by element-free galerkin methods. *Engineering Fracture Mechanics*, vol. 51, no. 2, pp. 295–315.

Belytschko, T.; Tabbara, M. (1996): Dynamic fracture using element-free galerkin methods. *International Journal for Numerical Methods in Engineering*, vol. 39, no. 6, pp. 923–938.

Besson, J.; Steglich, D.; Brocks, W. (2001): Modelling of crack growth in round bars and plane strain specimens. *International Journal of Solids and Structures*, vol. 38, pp. 8259–8284.

Chandra, N.; Shet, C. (2004): A micromechanistic perspective of cohesive zone approach in modeling fracture. *CMES: Computer Modeling in Engineering & Sciences*, vol. 5, no. 1, pp. 21–33.

Chen, J.-S.; Wu, C.-T.; Yoon, S.; You, Y. (2001): A stabilized conforming nodal integration for galerkin mesh-free method. *International Journal for Numerical Methods in Engineering*, vol. 50, pp. 435–466.

Chen, Z.; Gan, Y.; Chen, J. (2008): A coupled thermo-mechanical model for simulating the material failure evolution due to localized heating. *CMES: Computer Modeling in Engineering & Sciences*, vol. 26, no. 2, pp. 123–137.

Chu, C.; Needleman, A. (1980): Void nucleation effects in biaxially stretched sheets. *Journal of Engineering Materials and Technology*, vol. 102, pp. 249–256.

Duarte, C.; Oden, J. (1996): An h-p adaptive method using clouds. *Computer Methods in Applied Mechanics and Engineering*, vol. 139, pp. 237–262.

Fleming, M.; Chu, Y.; Moran, B.; Belytschko, T. (1997): Enriched element-free galerkin methods for crack tip fields. *International Journal for Numerical Methods in Engineering*, vol. 40, pp. 1483–1504.

Fujimoto, T.; Nishioka, T. (2006): Numerical simulation of dynamic elasto visco-plastic fracture using moving finite element method. *CMES: Computer Modeling in Engineering & Sciences*, vol. 11, no. 2, pp. 91–101.

Gao, L.; Liu, K.; Liu, Y. (2006): Applications of mlpg method in dynamic fracture problems. *CMES: Computer Modeling in Engineering & Sciences*, vol. 12, no. 3, pp. 181–195.

Gao, L.; Liu, K.; Liu, Y. (2006): Applications of mlpg method in dynamic fracture problems. *CMES: Computer Modeling in Engineering & Sciences*, vol. 12, no. 3, pp. 181–195.

Gunther, F.; Liu, W. (1998): Implementation of boundary conditions for meshless methods. *Computer Methods in Applied Mechanics and Engineering*, vol. 163, pp. 205–230.

Guo, Y.; Nairn, J. (2006): Three-dimensional dynamic fracture analysis using the material point method. *CMES: Computer Modeling in Engineering & Sciences*, vol. 16, no. 3, pp. 141–155.

Guo, Y.; Nairn, J. (2006): Three-dimensional dynamic fracture analysis using the material point method. *CMES: Computer Modeling in Engineering & Sciences*, vol. 16, no. 3, pp. 141–155.

Gurson, A. (1977): Continuum theory of ductile rupture by void nucleation and growth: part 1-yield criteria and flow rules for porous ductile media. *ASME Journal of Engineering Materials and Technology*, vol. 99.

Guz, A.; Menshykov, O.; Zozulya, V. (2007): Contact problem for the flat elliptical crack under normally incident shear wave. *CMES: Computer Modeling in Engineering & Sciences*, vol. 17, no. 3, pp. 205–214.

Hagihara, S.; Tsunori, M.; Ikeda, T. (2007): Application of meshfree method to elastic-plastic fracture mechanics parameter analysis. *CMES: Computer Modeling in Engineering & Sciences*, vol. 17, no. 2, pp. 63–72.

Han, Z.; Atluri, S. (2003): Truly meshless local petrov-galerkin (mlpg) solutions of traction and displacement bies. *Computations and Modelling in Engineering and Sciences*, vol. 4, pp. 665–678.

Hao, S.; Liu, W. (2006): Moving particle finite element method with superconvergence: Nodal integration formulation and applications. *Computer Methods in Applied Mechanics and Engineering*, vol. 195, no. 44-47, pp. 6059–6072.

Hao, S.; Liu, W.; Chang, C. (2000): Computer implementation of damage models by finite element and meshfree methods. *Computer Methods in Applied Mechanics and Engineering*, vol. 187, no. 3-4, pp. 401–440.

Hao, S.; Liu, W.; Klein, P.; Rosakis, A. (2004): Modeling and simulation of intersonic crack growth. *International Journal of Solids and Structures*, vol. 41, no. 7, pp. 1773–1799.

Hughes, T.; Winget, J. (1980): Finite rotation effects in numerical integration of rate constitutive equations arising in large-deformation analysis. *International Journal for Numerical Methods in Engineering*, vol. 15, pp. 1862–1867.

Idelsohn, S.; Onate, E. (2006): To mesh or not to mesh. that is the question... *Computer Methods in Applied Mechanics and Engineering*, vol. 195, pp. 4681–4696.

Joyce, J.; Hacket, E. (1994): Development of an engineering definition of the extent of j-controlled crack growth. *In Defect Assessment of Components-Fundamentals and Application, ESIS/EGF9, Blaut JG, Schwalbe KH. (eds). Mechanical Engineering Publications: London*, pp. 233–249.

Joyce, J.; Link, R. (1994): Effects of constraint on upper shelf fracture toughness. *Fracture Mechanics In Newman Jr JC, Reuter WG, Underwood JH (eds), 26th vol., ASTM STP 1256. American Society for Testing Materials.*

Kikuchi, M. (2006): Dimple fracture simulation of fracture specimen under different constraint conditions. *CMES: Computer Modeling in Engineering & Sciences*, vol. 11, pp. 49–59.

Liu, H.; Han, Z.; Rajendran, A.; Atluri, S. (2006): Computational modeling of impact response with the rg damage model and the meshless local petrov-galerkin (mlpg) approaches. *CMC: Computers Materials and Continua*, vol. 4, pp. 43–53.

Liu, W.; Hao, S.; Belytschko, T. (1999): Multiple scale meshfree methods for damage fracture and localization. *Computational Material Science*, vol. 16, no. 1-4, pp. 197–205.

Liu, W.; Jun, S.; Zhang, Y. (1995): Reproducing kernel particle methods. *International Journal for Numerical Methods in Engineering*, vol. 20, pp. 1081–1106.

Liu, W.; Jun, S.; Zhang, Y. (1995): Reproducing kernel particle methods. *International Journal for Numerical Methods in Engineering*, vol. 20, pp. 1081–1106.

Ma, J.; Lu, H.; Wang, B. (2006): Multiscale simulation using generalized interpolation material point (gimp) method and molecular dynamics (md). *CMES: Computer Modeling in Engineering & Sciences*, vol. 14, no. 2, pp. 101–117.

Maiti, S.; Geubelle, P. (2004): Mesoscale modeling of dynamic fracture of ceramic materials. *CMES: Computer Modeling in Engineering & Sciences*, vol. 5, no. 2, pp. 91–101.

Mc Clintock, F. (1968): A criterion for ductile fracture by the growth of holes. *Journal of Applied Mechanics*, vol. 35, pp. 363–371.

Melenk, J. M.; Babuska, I. (1996): The partition of unity finite element method: basic theory and applications. *Computer Methods in Applied Mechanics and Engineering*, vol. 139, pp. 289–314.

Miers LS, T. J. (2006): On the ngf procedure for lbie elastostatic fracture mechanics. *CMES: Computer Modeling in Engineering & Sciences*, vol. 14, no. 3, pp. 161–169.

Nishioka, T. (2005): Recent advances in numerical simulation technologies for various dynamic fracture phenomena. *CMES: Computer Modeling in Engineering & Sciences*, vol. 10, no. 3, pp. 209–215.

Nishioka, T.; Kobayashi, Y.; Fujimoto, T. (2007): The moving finite element method based on delaunay automatic triangulation for fracture path prediction simulations in nonlinear elastic-plastic materials. *CMES: Computer Modeling in Engineering & Sciences*, vol. 17, no. 3, pp. 231–238.

Organ, D.; Fleming, M.; Terry, T.; Belytschko, T. (1996): Continuous meshless approximations for nonconvex bodies by diffraction and transparency. *Computational Mechanics*, vol. 18, pp. 225–235.

Pardoen, T.; Hutchinson, J. (2000): An extended model for void growth and coalescence. *Journal of the Mechanics and Physics of Solids*, vol. 48, pp. 2467–2512.

Rabczuk, T.; Areias, P. (2006): A meshfree thin shell for arbitrary evolving cracks based on an extrinsic basis. *CMES: Computer Modeling in Engineering & Sciences*, vol. 16, no. 2, pp. 115–130.

Rabczuk, T.; Areias, P.; Belytschko, T. (2007): A meshfree thin shell method for non-linear dynamic fracture. *International Journal for Numerical Methods in Engineering*, vol. 72, no. 5, pp. 524–548.

Rabczuk, T.; Belytschko, T. (2004): Cracking particles: A simplified meshfree method for arbitrary evolving cracks. *International Journal for Numerical Methods in Engineering*, vol. 61, no. 13, pp. 2316–2343.

Rabczuk, T.; Belytschko, T. (2005): Adaptivity for structured meshfree particle methods in 2d and 3d. *International Journal for Numerical Methods in Engineering*, vol. 63, no. 11, pp. 1559–1582.

Rabczuk, T.; Belytschko, T. (2006): Application of particle methods to static fracture of reinforced concrete structures. *International Journal of Fracture*, vol. 137, no. 1-4, pp. 19–49.

Rabczuk, T.; Belytschko, T. (2007): A three dimensional large deformation meshfree method for arbitrary evolving cracks. *Computer Methods in Applied Mechanics and Engineering*, vol. 196, pp. 2777–2799.

Rabczuk, T.; Belytschko, T.; Xiao, S. (2004): Stable particle methods based on lagrangian kernels. *Computer Methods in Applied Mechanics and Engineering*, vol. 193, pp. 1035–1063.

Rabczuk, T.; Eibl, J. (2003): Simulation of high velocity concrete fragmentation using sph/mlsph. *International Journal for Numerical Methods in Engineering*, vol. 56, pp. 1421–1444.

Rabczuk, T.; PMA, P. A.; Belytschko, T. (2007): A simplified mesh-free method for shear bands with cohesive surfaces. *International Journal for Numerical Methods in Engineering*, vol. 69, no. 5, pp. 993–1021.

Rabczuk, T.; Zi, G. (2007): A meshfree method based on the local partition of unity for cohesive cracks. *Computational Mechanics*, vol. 39, no. 6, pp. 743–760.

Randles, P.; Libersky, L. (2000): Normalized sph with stress points. *International Journal for Numerical Methods in Engineering*, vol. 48, pp. 1445–1461.

Rice, J.; Tracey, D. (1969): On the ductile enlargement of voids in triaxial stress fields. *Journal of the Mechanics and Physics of Solids*, vol. 17, pp. 201–217.

Roy, Y.; Jr, R. D. (2002): Simulation of ductile crack growth in thin aluminum panels using 3-d surface cohesive elements. *International Journal of Fracture*, vol. 110, pp. 21–45.

Roychowdhury, S.; Roy, Y.; Jr, R. D. (2002): Ductile tearing in thin aluminum panels: experiments and analysis using large displacement, 3-d surface cohesive elements. *International Journal of Solids and Structures*, vol. 69, pp. 983–1002.

Rubenstein, R.; Atluri, S. (1983): Objectivity of incremental constitutive relations over finite time steps in computational finite deformation analysis. *Computer Methods in Applied Mechanics and Engineering*, vol. 36, pp. 277–290.

Tang, Z.; Shen, S.; Atluri, N. (2003): Analysis of materials with strain-gradient effects: A meshless local Petrov-Galerkin(mlpg) approach, with nodal displacements only. *CMES: Computer Modelling in Engineering and Sciences*, vol. 4, pp. 177–196.

Tvergaard, V. (1981): Influence of voids on shear band instabilities under plane strain condition. *International Journal of Fracture Mechanics*, vol. 17, pp. 389–407.

Tvergaard, V. (1982): On localization in ductile materials containing spherical voids. *International Journal of Fracture Mechanics*, vol. 18, pp. 237–252.

Tvergaard, V. (1990): Material failure by void growth to coalescence. *Advances in Applied Mechanics*, vol. 27, pp. 83–151.

Tvergaard, V.; Needleman, A. (1984): Analysis of the cup-cone fracture in a round tensile bar. *Acta Metallurgica*, vol. 32, pp. 157–169.

Ventura, G.; Xu, J.; Belytschko, T. (2002): A vector level set method and new discontinuity approximation for crack growth by efg. *International Journal for Numerical Methods in Engineering*, vol. 54, no. 6, pp. 923–944.

Wen, P.; Aliabadi, M.; Lin, Y. (2008): Meshless method for crack analysis in functionally graded materials with enriched radial base functions. *CMES: Computer Modeling in Engineering & Sciences*, vol. 30, no. 3, pp. 133–147.

Wen, P.; Hon, Y. (2007): Geometrically nonlinear analysis of reissner-mindlin plate by meshless computation. *CMES: Computer Modeling in Engineering & Sciences*, vol. 21, pp. 177–191.

Wu, X.; Tao, S. S. W. (2007): Meshless local petrov-galerkin collocation method for two-dimensional heat conduction problems. *CMES: Computer Modeling in Engineering & Sciences*, vol. 22, pp. 65–76.

Xia, L.; Shih, F. (95): Ductile crack growth-i. a numerical study using computational cells with microstructurally based length scales. *Journal of the Mechanics and Physics of Solids*, vol. 43, pp. 233–259.

Xia, L.; Shih, F. (95): Ductile crack growth-ii. void nucleation and geometry effects on macroscopic fracture behaviour. *Journal of the Mechanics and Physics of Solids*, vol. 43, pp. 1953–1981.

Xia, L.; Shih, F.; Hutchinson, J. (1995): A computational approach to ductile crack growth under large scale yielding conditions. *Journal of the Mechanics and Physics of Solids*, vol. 43, pp. 389–413.

Xu, S.; Dong, Y.; Zhang, Y. (2008): An efficient model for crack propagation. *CMES: Computer Modeling in Engineering & Sciences*, vol. 30, no. 1, pp. 17–26.

You, Y.; Chen, J.; Voth, T. (2002): Characteristics of semi- and full discretization of stabilized galerkin meshfree method. *Finite Elements in Analysis and Design*, vol. 38, pp. 999–1012.

Zhang, Y.; Chen, L. (2008): A simplified meshless method for dynamic crack growth. *CMES: Computer Modeling in Engineering & Sciences*, vol. 31, no. 3, pp. 189–199.